I&EC research
Industrial & Engineering Chemistry Research

pubs.acs.org/IECR

Article

Shelter for Biologically Relevant Molecules: Photoprotection and Enhanced Thermal Stability of Folic Acid Loaded in a ZIF-8 MOF Porous Host

Jimena S. Tuninetti,[‡] Mariana P. Serrano,[‡] Andrés H. Thomas, Omar Azzaroni, and Matías Rafti*

Cite This: https://dx.doi.org/10.1021/acs.iecr.0c04905

Read Online

ACCESS | Metrics & More | Article Recommendations | Supporting Information

ABSTRACT: We hereby propose the use of ZIF-8 MOF (a biocompatible porous material belonging to the zeolitic imidazolate framework subclass) as a host for biologically relevant molecules such as folic acid (PteGlu). It was demonstrated that PteGlu loading can be achieved *via* a straightforward one-pot encapsulation procedure without compromising the ZIF-8 crystalline structure, given that suitable molar ratios of the metal precursor, linker, and guest molecule are employed. The PteGlu@ZIF-8 composite thus synthesized brings two novel interesting features: increased thermal stability and a remarkable photoprotection effect of the highly photolabile PteGlu molecule. Both features are very relevant for common uses of PteGlu, such as the production of folate-enriched food.

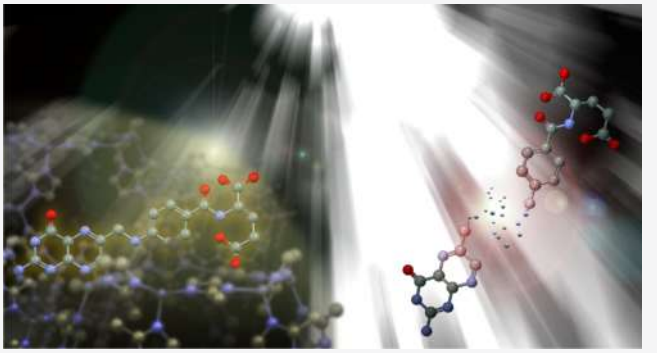

INTRODUCTION

The term metal−organic frameworks (MOFs) refers to a class of porous materials that can feature relatively high chemical and thermal stability. MOFs can be described as infinite coordination networks built upon metal ions (or metal clusters) and multidentate organic linkers, binding usually through carboxylic or heterocyclic nitrogen moieties.[1−3] Among the key features that make MOFs appealing candidates for selective adsorption and drug delivery applications are the high surface areas and pore volumes available and the wide chemical versatility possible by positioning selected moieties on the pore walls.[4−7] In the past few decades, *ad hoc* design of MOFs and composites including MOFs was successfully employed for numerous remarkable applications, *e.g.*, heterogeneous catalysis (with embedded metal nanoparticles as active sites),[8,9] luminescence and optoelectronics,[10,11] drug delivery,[12,13] and impedimetric sensing (enabled by the incorporation of conducting elements).[14,15]

Zeolite imidazolate frameworks or ZIFs (a MOF subclass named after their zeolite-like topologies) are constituted by tetrahedrally coordinated Co^{2+} or Zn^{2+} metallic centers with imidazolate *N*-bidentate linkers.[16] A prominent member of this subclass is ZIF-8 (also available commercially as BASOLITE-Z1200 manufactured by BASF) based on zinc ions and 2-methyl-imidazolate linker. The use of ZIF-8 was extensively reported for diverse applications due to interesting properties such as good biocompatibility and mechanical robustness.[17,18] Additionally, ZIF-8 can be synthesized using inexpensive solvents and mild conditions (*i.e.*, room temperature and relatively cheap zinc salts with water or methanol as a solvent) and features considerably high Brunauer−Emmett−Teller (BET) surface areas (above 1000 m^2/g), with 3.4 Å windows and 11.6 Å diameter micropores.[19] Among the most relevant reports to the present study, the use of ZIF-8 for food safety control and drug delivery with caffeine as a model adsorbate should be mentioned.[20,21] In an interesting contribution, Zhuang et al. discussed the use of ZIF-8 as a carrier for camptothecin, an anticancer drug that can be loaded by simple direct mixing with MOF precursors.[22] These examples, together with many studies in which enzymes were shown to remain active upon encapsulation, demonstrate that MOF can act as a suitable scaffold, providing enhanced stability and preserved functionality.[23−26] Pteroyl-L-glutamic acid (widely known as folic acid and hereafter referred to as PteGlu), is a soluble vitamin essential for mammals. The chemical structure of PteGlu can be breakdown into three parts: 6-methylpterin (Mep), *p*-aminobenzoic acid (PABA), and a glutamic acid residue (Glu) (see Scheme 1). In living systems, PteGlu is present in multiple forms including molecules with several glutamate residues and di- or tetra-hydro derivatives. This large group of related compounds is known as folates. Tetrahy-

Received: October 6, 2020
Revised: October 29, 2020
Accepted: October 30, 2020

Scheme 1. Molecular Structure of Pteroyl-L-glutamic Acid (PteGlu)

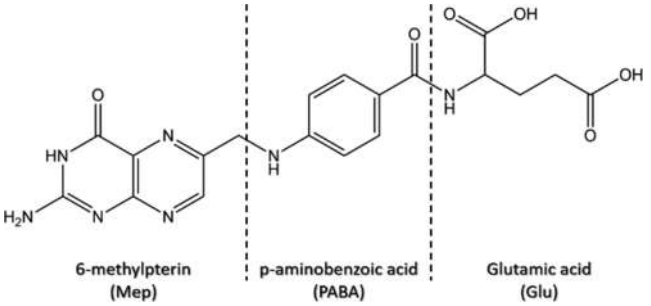

drofolate and its derivatives act as coenzymes in one-carbon transfer reactions in mammals, leading to the synthesis of essential biomolecules such as proteins and nucleic acids.[27] Folate deficiency is related to important health disorders, among them are megaloblastic anemia, pregnancy complications, and neural tube defects,[28,29] which led to the implementation of food regulations to ensure an adequate intake, especially for women in childbearing age. The most widely used folate source is PteGlu due to its cost-effectiveness, relatively high stability, and straightforward metabolization into biologically active derivatives such as 5-methyltetrahydrofolic acid.[30] A common drawback for the use of all naturally occurring folates (including PteGlu) is their high susceptibility toward degradation in common conditions, such as oxygen-containing solutions, low pH values, high temperatures, and, mainly, upon exposure to ultraviolet (UV) radiation due to UV-B (280−320 nm) and UV-A (320−400 nm) absorption bands.[31,32] Such susceptibility compromises PteGlu integrity, and thus, even when embedded in protective matrices, bioavailability can be lost if not properly stored and managed.[33]

PteGlu constitutes a model system for the study of photodegradation of folates, and many reports describe photochemical processes occurring in aqueous environments and other solvents.[34,35] In oxygen-free aqueous solutions, PteGlu remains photostable, but its excitation in the presence of molecular oxygen leads to cleavage and oxidation reactions, producing 6-formylpterin (Fop) and *p*-aminobenzoylglutamic acid (PABA-Glu) as main photoproducts (see Scheme 2). Upon further irradiation, Fop is subsequently converted into 6-carboxypterin (Cap) and pterin (Ptr).

Having in mind the above-discussed ideas on the possibilities enabled by versatile porous materials like MOFs acting as hosts (with triggered disassembly upon exposure to *in vivo* conditions)[36] and the need for improving PteGlu stability after loading in biocompatible matrices, we envisioned the feasibility of ZIF-8 MOF for such end using the already reported one-pot encapsulation approach.[37] Although there have been some recent related reports, specifically, on the use of MOFs[38−42] and cyclodextrins[43] for synthesizing PteGlu composites, a crucial point remains yet virtually unexplored, *i.e.*, the assessment of the potential photoprotective effect on the photolabile PteGlu molecule. Along this line of thought, a recent report by Pagano et al. demonstrates that spatial confinement through Zn-carboxylate intercalation complexes of PteGlu in lamellar double hydroxides (LDHs, anionic layered clays) is capable of photoprotection, thus potentially advantageous for the formulation of novel skin care products containing PteGlu.[44] We addressed this point further for PteGlu@ZIF-8 by carrying a thorough characterization that resulted in the demonstration of a remarkable photoprotective effect. Moreover, the ZIF-8 matrix enables high PteGlu loadings and also provides an enhancement of thermal stability, highly relevant for the production of folate-enriched food.[45]

EXPERIMENTAL SECTION

Chemicals. Methanol (CH_3OH Anedra, RA-ACS), zinc nitrate hexahydrate ($Zn(NO_3)_2{\cdot}6H_2O$, Sigma-Aldrich, 98%), 2-methylimidazole ($C_4H_6N_2$, Aldrich, 99%), ethylenediaminetetraacetic acid (EDTA, ICN Biomedicals Inc.), and sodium hydroxide (Anedra, 98.6%) were used for the experiments hereby described without further purification. Pteroyl-L-glutamic acid (PteGlu) and other pterin derivatives were provided by Schircks Laboratories (purity >98.5%). Ammonium acetate (NH_4Ac) was purchased from Sigma.

ZIF-8 Synthesis. ZIF-8 stock colloidal suspensions were synthesized by mixing 12.5 mL of 50 mM methanolic zinc nitrate and 12.5 mL of 50 mM 2-methylimidazole methanolic at room temperature. After the reaction, the product was purified by repeated solvent exchange cycles.

PteGlu@ZIF-8 Synthesis. PteGlu encapsulated in ZIF-8 was synthesized with slightly modified procedures based on recent reports. Special care was taken in ensuring the preservation of PteGlu exposure to light sources.[37] PteGlu and zinc nitrate methanolic solutions were mixed to promote the interaction between Zn^{2+} and carboxylic moieties on the glutamate residue; such a premixing step was demonstrated to

Scheme 2. Photo-oxidation of PteGlu in Air-Equilibrated Aqueous Solutions under UV-A Irradiation

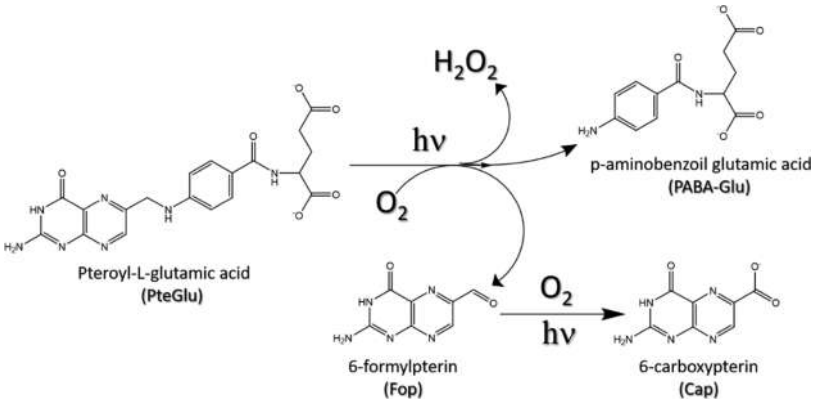

https://dx.doi.org/10.1021/acs.iecr.0c04905
Ind. Eng. Chem. Res. XXXX, XXX, XXX−XXX

trigger confined nucleation due to supersaturation upon the addition of 2-methylimidazolate linker (see Fourier transform infrared (FTIR) spectroscopy experiments below).[46,47] Briefly, 12.5 mL of 50 mM methanolic zinc nitrate solution was mixed with 12.5 mL of methanol with 12.0 mg of PteGlu dissolved in 12.5 mL of methanol in the absence of light for a 7:1 molar ratio (zinc/PteGlu). The as-prepared mixture was sonicated in a cold bath for 20 min and then mixed at room temperature with 12.5 mL of 50 mM 2-methylimidazole methanolic solution (equimolar metal/linker molar ratio, total volume 37.5 mL). The obtained yellowish-orange suspension (see the Supporting Information, Figure S1) was purified by repeated cycles of precipitation and solvent exchange with deionized water (DIW), then resuspended in DIW, and kept away from light for further characterization regarding PteGlu loading, crystal structure, particle size and morphology, porosity, and chemical structure. For experiments exploring the effect of high PteGlu molar ratios on the material obtained, PteGlu solutions were prepared with 24.0 mg of PteGlu dissolved in 12.5 mL of methanol.

Wide-Angle X-ray Scattering (WAXS). The crystalline structure was assessed with wide-angle X-ray scattering (WAXS) measurements on powdered samples. The equipment used for small-angle X-ray scattering (SAXS)/WAXS (IN-IFTA, "Nanopymes"-EuropeAid/132184 D/SUP/AR Contract 331-896) is a XEUSS 1.0 HR (XENOCS, Grenoble) equipped with a microfocus X-ray source and a PILATUS 100 K detector (DECTRIS AG, Switzerland).

Transmission Electron Microscopy (TEM). Transmission electron microscopy experiments were carried out with a JEOL 1200 EXII 120 kV transmission electron microscope equipped with a Gatan Orius Digital 2k × 2k CCD camera.

N_2 Sorption Isotherms. N_2 sorption isotherms at 77 K were assessed with a Micromeritics accelerated surface area and porosimeter analyzer, ASAP 2020. Adsorption−desorption isotherms were analyzed to achieve characterization in terms of the Brunauer−Emmett−Teller (BET) surface area, pore size, and pore volume.

Fourier Transform Infrared (FTIR) Spectroscopy. A Varian 660-IR apparatus in transmission mode was used to characterize the obtained materials after inclusion in KBr pellets.

Thermogravimetric Analysis (TGA). Thermal degradation of synthesized materials was assessed using a TA Instruments equipment (TGA Q500). All samples were subjected to heating rates of 10 °C/min under a 40 mL/min N_2 flux.

Steady-State Photolysis Experiments. Continuous photolysis experiments of PteGlu and PteGlu@ZIF-8 were carried by irradiating 1 mL of samples of air-equilibrated aqueous suspensions of PteGlu@ZIF-8 (0.7 mg/mL−10% PteGlu) and 150 μM aqueous solutions of PteGlu (identical concentration based on the PteGlu loading determined, see TGA experiments below), respectively, using quartz cells (1 cm optical path length) under continuous magnetic stirring at room temperature. A triplicate series of experiments were carried out in each case, and results obtained for each irradiation period correspond to an independent sample from the same PteGlu@ZIF-8 synthesis batch. The irradiation setup used consists of a Rayonet RPR 3500 lamp (Southern N.E. Ultraviolet Co.) with emission centered at 350 nm (bandwidth 20 nm) as a radiation source, placed at 1 cm from the quartz cell. An Aberchrome 540 (Aberchromics Ltd.) was used as an actinometer for the incident photon flux density measurement ($q^{0,V}_{\lambda,p}$) at the excitation wavelength from the Rayonet RPR lamp. The method for the determination of $q^{0,V}_{\lambda,p}$ has been described in detail elsewhere.[48] The lamp irradiance was calculated using $q^{0,V}_{\lambda,p}$ value resulting in $E^{L}_{UV} = 16 \pm 2$ W/m^2.[49]

Once a prescribed irradiation period elapsed, samples were analyzed using high-performance liquid chromatography (HPLC) to detect the presence of photolysis products, this is necessary due to the similar absorption bands of the species involved as reactants and products, while for PteGlu solutions, direct injection into the separation column is possible; for the analysis of irradiated PteGlu@ZIF-8 suspensions, an additional step was required. After irradiation, each PteGlu@ZIF-8 sample was centrifuged at 13 000g for 30 min and the supernatant was removed. The ZIF-8 porous host was removed by exposing the pellet to 100 mM pH 10.0 EDTA solutions for 30 min at 25 °C while shaking at 1100 rpm (see the Supporting Information, Figure S4, where the effect on the host is depicted). Due to a strong affinity toward Zn^{2+} ions, EDTA causes MOF disassembly, leading to PteGlu liberation, which otherwise remains in the porous host even after long periods of exposure to aqueous environments, as demonstrated by complementary release experiments. A contact period of 7 days yields liberation of only approx. 10% of the total loaded PteGlu amount on the ZIF-8 host; *i.e.*, the liberation during the time span considered in the hereby discussed experiments can be neglected for all practical purposes (see the Supporting Information, Figure S7). All samples were filtered through a 0.20 μm Teflon filter prior to HPLC analysis.

HPLC Analysis of Irradiated Samples. A high-performance liquid chromatography (HLPC) Prominence from Shimadzu (solvent delivery module LC-20AT, on-line degasser DGU-20A5, communications bus module CBM-20, autosampler SIL-20A HT, column oven CTO-10AS VP, photodiode array detector SPD-M20A, and fluorescence (FL) detector RF-20A) was employed for monitoring photochemical processes. A Synergi Polar-RP column (ether-linked phenyl phase with polar end capping, 150 mm × 4.6 mm, 4 μm, Phenomenex) was used for product separation. Solutions containing 3% methanol and 97% 25 mM formic acid (pH 3.2) were used as the mobile phase. The column temperature was set to 25 °C, and the flow rate was fixed to 0.6 mL/min. Sodium acetate solution was used as the mobile phase (1 mM NH_4Ac, pH 6.7).

RESULTS AND DISCUSSION

Characterization of PteGlu@ZIF-8 Synthesized *via* a One-Pot Procedure. In Figure 1, the results obtained from characterization experiments carried on PteGlu@ZIF-8 are displayed. Diffractograms obtained *via* wide-angle X-ray scattering (WAXS) performed in solid samples (Figure 1A) are in line with what can be expected from the ZIF-8 reported structure. This demonstrates that PteGlu inclusion does not affect the MOF crystalline structure for the molar ratio used in the premixing step (ratio (Zn/PteGlu) = 1:7).[19] Further WAXS experiments (see the Supporting Information, Figure S2) suggest that higher PteGlu proportions causes the appearance of both the loss of the ZIF-8 crystalline structure and some degree of phase segregation, as demonstrated by additional diffraction peaks attributable to the PteGlu phase when premixing step was carried out using Zn/PteGlu = 1:14 molar ratio (although it can be expected that PteGlu loading on the composite material obtained using 1:14 molar ratio to

https://dx.doi.org/10.1021/acs.iecr.0c04905
Ind. Eng. Chem. Res. XXXX, XXX, XXX−XXX

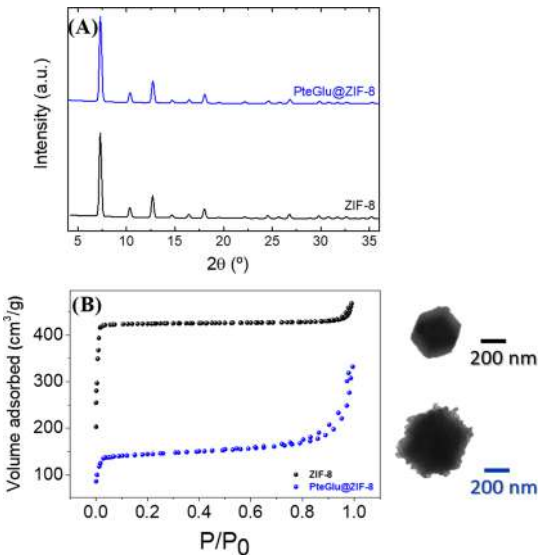

Figure 1. Characterization of composites obtained using the reactant mixture molar ratio (Zn/PteGlu) = 1:7. (A) WAXS of both ZIF-8 and PteGlu@ZIF-8 and (B) N_2 adsorption isotherms performed at 77 K for ZIF-8 (black) and PteGlu@ZIF-8 composite (blue), together with the corresponding TEM micrographs of the approx. 300−400 nm diameter nanocrystals.

be higher than the corresponding 1:7 ratio, due to the above-mentioned evidence of phase segregation, a direct comparison is not meaningful, among other factors because of the possible contribution to total PteGlu loading of molecules binding in ZIF-8 Zn-defect sites; see the Supporting Information, Figure S2).[50] TEM images of the obtained PteGlu@ZIF-8 nanoparticles display the typical hexagonal-shaped cross section, as presented in Figure 1B, similar to what is observed for bare ZIF-8, aside from slight size differences and the appearance of surface rugosity related to defects caused by the PteGlu presence (approx. 300−400 nm diameter, rhombic dodecahedra). The particle size distribution obtained for PteGlu@ZIF-8 is less monodisperse than that for bare ZIF-8, as shown in wide-field TEM images, see the Supporting Information, Figure S3. Calculated BET surface areas obtained from N_2 adsorption isotherms on bare ZIF-8 and PteGlu@ZIF-8 show remarkable differences. A value of 1210 m^2/g, which reduced to 416 m^2/g (≈65% surface area reduction) when PteGlu was included in the porous host, suggests a considerable occupation of the available pore space, as shown in Figure 1B. Additionally, a clear hysteresis loop for $0.8 < P/P_0 < 1$ relative pressure can be observed for PteGlu@ZIF-8, which is a hallmark of the presence of additional mesoporosity, in line with the surface roughening observed in TEM images.

Fourier transform infrared (FTIR) spectroscopy characterization was conducted to gain further insight into the nature of the interactions between PteGlu and ZIF-8 (Figure 2). It can be observed that PteGlu@ZIF-8 retains the absorption bands corresponding to vibrational modes present in ZIF-8, *e.g.*, 1580 cm^{-1} ascribed to C═N stretching, 1308 cm^{-1} ascribed to C−H imidazolate ring-bending mode, and both 1179 and 1145 cm^{-1} bands corresponding to C−N in-plane stretching.[51]

The above-discussed features confirm that moderate loadings of PteGlu on ZIF-8 do not cause a significant alteration on the host porous matrix. Regarding the comparison between PteGlu and PteGlu@ZIF-8, several interesting observations can be made. Typical PteGlu

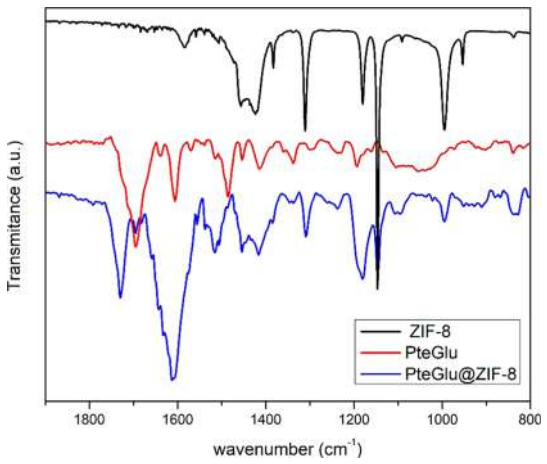

Figure 2. FTIR spectra for PteGlu (red), ZIF-8 (black), and PteGlu@ZIF-8 (blue).

absorption bands related to, namely, both symmetric and asymmetric C═O stretching modes (1700 and 1480 cm^{-1}, respectively); 6-methylpterin (Mep) aromatic ring stretching vibration (1620 cm^{-1}); acid moieties of the PABA ring (1420 cm^{-1}); and bands centered at 853, 1192, and 1297 cm^{-1} corresponding to the out-of-plane and in-plane $-NH_2$ vibrations and C−N stretching.[52] When comparing the position of the above-mentioned bands for PteGlu@ZIF-8, three striking differences can be individualized: (i) the band centered at 1620 cm^{-1} (Mep ring stretching) becomes more intense and broadens, (ii) the intensity of 1480 cm^{-1} asymmetric carboxylic C═O stretching band decreases, and (iii) the symmetric carboxylic C═O stretching band is blue-shifted from 1700 to 1730 cm^{-1}. The widening of the 1480 cm^{-1} vibrational band related to the Mep aromatic ring points toward some degree of spatial confinement of PteGlu on the porous host. The effect observed on symmetric/asymmetric stretching bands can be rationalized by considering general characteristics of coordination interactions between carboxylic moieties and metal ions (*e.g.*, Zn^{2+}).[53] It was demonstrated that not only peak positions are highly dependent on the chemical identity of carboxylic acid considered (*e.g.*, formate or acetate derived) but also, more interestingly, the intensity variation of asymmetric (strong absorption) and symmetric (moderate absorption) modes depends on the strength and type of metal−ligand interaction (*e.g.*, ionic, monodentate, bidentate). The observed changes in PteGlu IR spectra when loaded in the ZIF-8 host allow us to infer that coordination is likely to occur predominantly *via* monodentate coordination of Zn^{2+} ions with carboxylic moieties on the glutamic acid residue,[54] as expected, considering the wide variety of coordination compounds (including archetypal MOFs) based on Zn-carboxylate building blocks.[55]

Thermogravimetric Analysis (TGA) Experiments for Determination PteGlu Loading and Characterization of PteGlu@ZIF-8 Thermal Stability. The determination of PteGlu@ZIF-8 thermal stability was carried with TGA experiments under a N_2 atmosphere (Figure 3). The thermal stability of PteGlu (weight loss events starting at $T \approx 180$ °C) is substantially enhanced when loaded on ZIF-8 since PteGlu@ZIF-8 weight loss starts only at temperatures > 350 °C (thermal decomposition of ZIF-8 occurs at $T = 450$ °C in a N_2 atmosphere).[50,56,57] Such an enhancement can be understood by considering the above-discussed confinement of

https://dx.doi.org/10.1021/acs.iecr.0c04905
Ind. Eng. Chem. Res. XXXX, XXX, XXX−XXX

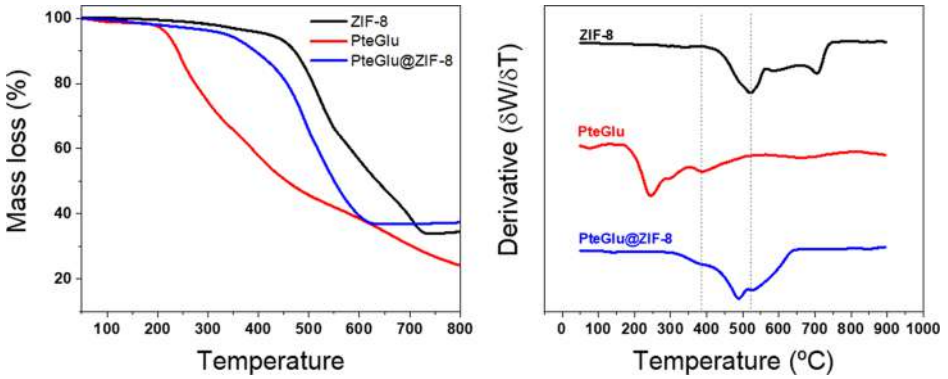

Figure 3. Thermogravimetric analysis in the N_2 atmosphere of ZIF-8 (black), PteGlu (red), and PteGlu@ZIF-8 (blue).

PteGlu within the ZIF-8 porous structure. Deconvolution of the superimposed thermal processes is not straightforward, but considering that for $T < 400$ °C ZIF-8 porous host remains stable, PteGlu contained in the composite can be estimated to be 10.0% w/w, in line with HPLC determinations carried out on the composite upon EDTA disassembly. This value corresponds to a resulting (Zn/PteGlu) molar ratio of 5.3:1, slightly lower than the 7:1 molar ratio used for the premixing step during the one-pot synthesis procedure.

Comparison of Bare and ZIF-8-Loaded PteGlu Photostability under UV-A Irradiation. Air-equilibrated aqueous suspensions of PteGlu@ZIF-8 were exposed to controlled UV-A irradiation, and after chemical removal of the ZIF-8 matrix (see Figure S4 and Experimental Section for more detailed information), the concentrations of PteGlu and possible photoproducts present were determined with the high-performance liquid chromatography (HPLC) technique (see Figures S5 and S6 and the Supporting Information for details on the procedure followed). Results were then compared to those of the control photolysis experiment carried out with bare PteGlu aqueous solutions under identical conditions; in line with previous reports, PteGlu was observed to undergo photo-oxidation, with Fop and PABA-Glu as products (see Figure 4A). Subsequent oxidation processes result in the appearance of Cap and eventually pterin. On the other hand, irradiation of PteGlu@ZIF-8 suspensions resulted in a remarkable photoprotective effect, as observed in Figure 4B; *i.e.*, after 15 min of irradiation, only less than 20% of PteGlu was consumed, in contrast to control experiments in which PteGlu was almost completely consumed after 5 min irradiation. Spontaneous liberation of PteGlu from the host can be regarded as negligible for the time range considered and conditions used in photolysis experiments, as demonstrated by control experiments (see the Supporting Information, Figure S7). Therefore, any photodegradation processes resulting from PteGlu radiation absorption can be considered to occur within the host porous matrix. An important factor that should be considered when comparing the irradiation of PteGlu solutions (homogeneous) and PteGlu@ZIF-8 (heterogeneous) is the scattering of radiation caused by colloidal particles present. That is, under identical irradiation conditions, the number of photons reaching PteGlu in aqueous solutions would be higher than that corresponding to colloidal suspensions of PteGlu@ZIF-8. The relevant parameters for estimating scattering radiation loss for a given wavelength and considering nonabsorbing colloidal particles are the optical density or concentration and the size/shape of such objects. A fair estimate of an upper limit value for this effect is ≈10−20%, considering 350 nm absorbance of bare ZIF-8 suspensions (0.7 mg/mL) (see the Supporting Information, Figure S4).[58,59] Even after considering such radiation losses, the photoprotection effect is still remarkable, with 80% reduction in PteGlu consumption when hosted in the host matrix after 15 min of irradiation.

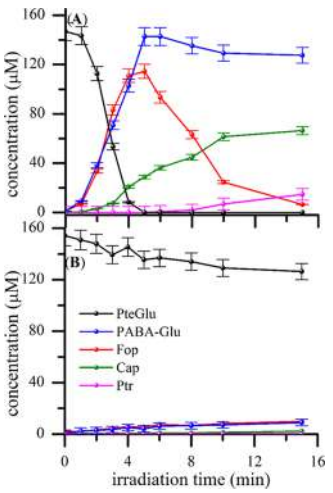

Figure 4. Time evolution of reactant and photoproduct concentrations, determined by HPLC analysis, of (A) air-equilibrated aqueous solutions of PteGlu and (B) air-equilibrated aqueous suspensions of PteGlu@ZIF-8 under UV-A irradiation. $[PteGlu]_0$ = 155 μM, pH = 6.0. λ_{irr} = 350 nm.

The acceleration observed for free PteGlu consumption as the reaction time proceeds (Figure 4A) can be explained by taking into account the already reported autocatalytic photosensitization processes caused by photoproducts.[35] Recent reports dealing with the effect of pterinic impurities on PteGlu photostability suggest that degradation does not proceed by direct excitation of the pterinic moiety but by photosensitization with unconjugated pterins present as impurities, particularly Fop and Cap.[30] Surprisingly, such typical behavior was not observed upon irradiation of PteGlu@ZIF-8 suspensions.

To gain further insight into the photosensitized oxidation of PteGlu by unconjugated pterins in the ZIF-8 matrix, a series of experiments were performed by adding Fop to PteGlu@ZIF-8 suspensions. In these experiments, the initial concentration of Fop was 30 μM, and under such conditions, PteGlu consumption proceeds as a result of photosensitization by

https://dx.doi.org/10.1021/acs.iecr.0c04905
Ind. Eng. Chem. Res. XXXX, XXX, XXX−XXX

Fop rather than through direct photolysis of PteGlu. HPLC concentration profiles obtained reveal that upon irradiation of air-equilibrated PteGlu solutions containing Fop, PteGlu was rapidly oxidized, while the addition of Fop to PteGlu@ZIF-8 suspensions had a negligible effect on the PteGlu consumption rate (Figure 5). This interesting result suggests that PteGlu

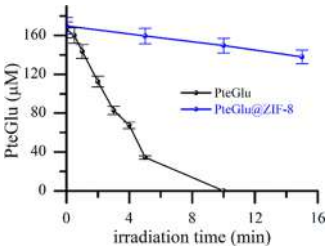

Figure 5. Time evolution of PteGlu concentration in air-equilibrated aqueous solutions of PteGlu and suspensions of PteGlu@ZIF-8 under UV-A irradiation in the presence of Fop. $[PteGlu]_0$ = 168 μM, $[Fop]_0$ = 30 μM, pH = 5.5. λ_{irr} = 350 nm.

loading on ZIF-8 causes an enhancement on photostability, even in the presence of unconjugated pterins known to accelerate such processes.

CONCLUSIONS

We have synthesized PteGlu@ZIF-8 by a simple one-pot encapsulation method that yields high loadings of such a biologically relevant molecule in a biocompatible high-surface-area host porous matrix. Thorough characterization of the obtained material demonstrated that the ZIF-8 crystalline structure and porosity remains present upon encapsulation of PteGlu. Given the relative sizes of the ZIF-8 pore window and diameter and PteGlu molecular dimensions, it is unlikely that a postsynthetic loading procedure would yield an integrated composite like that presented herein. We hypothesize that the premixing step, in which metal precursor coordination with carboxylic acid moieties present on PteGlu occurs, plays a crucial role in the structuration of clusters, which later on develop into the highly integrated composite particles. Evidence of the enhancement of PteGlu thermal stability caused by confinement constitutes a desirable feature having in mind the requirements of potential applications, involving exposure to high temperatures (*e.g.*, sterilization procedures or food processing). Although such a thermal protection effect was already observed for other edible biocompatible hosts, the use of ZIF-8 MOF allows enhanced maximum temperature limits and higher loadings (10% w/w).[43,60−62] Another interesting feature of the encapsulation of PteGlu on PteGlu@ZIF-8 is the photoprotection effect, which provokes a remarkable increase in stability toward irradiation with UV-A sources compared to free PteGlu (up to 80% increase). Although some radiation loss due to scattering must be considered; based on photosensitization experiments carried out with the addition of Fop, we hypothesize that the photoprotection mechanism involves a separation of PteGlu and whatever trace Fop amounts produced in the early stages of the irradiation process, which although difficult to detect can greatly accelerate the autocatalytic degradation process. It should be mentioned also a possible contribution to the observed photoprotection arising from Zn-carboxylate complexes, which were shown to be more stable than free PteGlu. In summary, the hereby proposed biocompatible porous matrix is suitable for loading of a biologically relevant molecule such as PteGlu, yields enhanced thermal stability and photostability, and also offers the interesting possibility of triggered disassembly upon exposure to *in vivo* conditions.

ASSOCIATED CONTENT

Supporting Information

The Supporting Information is available free of charge at https://pubs.acs.org/doi/10.1021/acs.iecr.0c04905.

Further characterization of the synthesized materials including TEM, X-ray diffraction, and UV−vis absorption spectrum of the species involved in the discussed photochemical processes (PDF)

AUTHOR INFORMATION

Corresponding Author

Matías Rafti − *Instituto de Investigaciones Fisicoquímicas Teóricas y Aplicadas, Departamento de Química, Facultad de Ciencias Exactas, Universidad Nacional de La Plata, CONICET, La Plata B1904DPI, Argentina;* orcid.org/0000-0003-3393-358X; Email: mrafti@quimica.unlp.edu.ar

Authors

Jimena S. Tuninetti − *Instituto de Investigaciones Fisicoquímicas Teóricas y Aplicadas, Departamento de Química, Facultad de Ciencias Exactas, Universidad Nacional de La Plata, CONICET, La Plata B1904DPI, Argentina;* orcid.org/0000-0002-9813-1265

Mariana P. Serrano − *Instituto de Investigaciones Fisicoquímicas Teóricas y Aplicadas, Departamento de Química, Facultad de Ciencias Exactas, Universidad Nacional de La Plata, CONICET, La Plata B1904DPI, Argentina;* orcid.org/0000-0002-2476-6794

Andrés H. Thomas − *Instituto de Investigaciones Fisicoquímicas Teóricas y Aplicadas, Departamento de Química, Facultad de Ciencias Exactas, Universidad Nacional de La Plata, CONICET, La Plata B1904DPI, Argentina;* orcid.org/0000-0002-8054-7799

Omar Azzaroni − *Instituto de Investigaciones Fisicoquímicas Teóricas y Aplicadas, Departamento de Química, Facultad de Ciencias Exactas, Universidad Nacional de La Plata, CONICET, La Plata B1904DPI, Argentina;* orcid.org/0000-0002-5098-0612

Complete contact information is available at: https://pubs.acs.org/10.1021/acs.iecr.0c04905

Author Contributions

‡J.S.T. and M.P.S. contributed equally to this work.

Notes

The authors declare no competing financial interest.

ACKNOWLEDGMENTS

This work was supported by CONICET (PUE 2017 22920170100100CO), ANPCyT (PICT 2018-00780, PICT 2017-0925), and UNLP (11/X840). M.P.S., J.S.T., M.R., A.T., and O.A. are staff researchers of CONICET.

REFERENCES

(1) Hoskins, B. F.; Robson, R. Infinite Polymeric Frameworks Consisting of Three Dimensionally Linked Rod-like Segments. *J. Am. Chem. Soc.* **1989**, *111*, 5962−5964.

(2) Yaghi, O. M.; Li, H.; Davis, C.; Richardson, D.; Groy, T. L. Synthetic Strategies, Structure Patterns, and Emerging Properties in the Chemistry of Modular Porous Solids†. *Acc. Chem. Res.* **1998**, *31*, 474−484.
(3) Batten, S. R.; Champness, N. R.; Chen, X. M.; Garcia-Martinez, J.; Kitagawa, S.; Öhrström, L.; O'Keeffe, M.; Suh, M. P.; Reedijk, J. Terminology of Metal-Organic Frameworks and Coordination Polymers (IUPAC Recommendations 2013). *Pure Appl. Chem.* **2013**, *85*, 1715−1724.
(4) Li, J. R.; Ma, Y.; McCarthy, M. C.; Sculley, J.; Yu, J.; Jeong, H. K.; Balbuena, P. B.; Zhou, H. C. Carbon Dioxide Capture-Related Gas Adsorption and Separation in Metal-Organic Frameworks. *Coord. Chem. Rev.* **2011**, *255*, 1791−1823.
(5) Li, J.; Wang, X.; Zhao, G.; Chen, C.; Chai, Z.; Alsaedi, A.; Hayat, T.; Wang, X. Metal-Organic Framework-Based Materials: Superior Adsorbents for the Capture of Toxic and Radioactive Metal Ions. *Chem. Soc. Rev.* **2018**, *47*, 2322−2356.
(6) Ma, S.; Zhou, H. C. Gas Storage in Porous Metal-Organic Frameworks for Clean Energy Applications. *Chem. Commun.* **2010**, *46*, 44−53.
(7) Suh, M. P.; Park, H. J.; Prasad, T. K.; Lim, D. W. Hydrogen Storage in Metal-Organic Frameworks. *Chem. Rev.* **2012**, *112*, 782−835.
(8) Gascon, J.; Corma, A.; Kapteijn, F.; Llabrés i Xamena, F. X. Metal Organic Framework Catalysis: Quo Vadis? *ACS Catal.* **2014**, *4*, 361−378.
(9) Farrusseng, D.; Aguado, S.; Pinel, C. Metal−Organic Frameworks: Opportunities for Catalysis. *Angew. Chem., Int. Ed.* **2009**, *48*, 7502−7513.
(10) Kreno, L. E.; Leong, K.; Farha, O. K.; Allendorf, M.; Van Duyne, R. P.; Hupp, J. T. Metal−Organic Framework Materials as Chemical Sensors. *Chem. Rev.* **2012**, *112*, 1105−1125.
(11) Stavila, V.; Talin, A. A.; Allendorf, M. D. MOF-Based Electronic and Opto-Electronic Devices. *Chem. Soc. Rev.* **2014**, *43*, 5994−6010.
(12) Horcajada, P.; Gref, R.; Baati, T.; Allan, P. K.; Maurin, G.; Couvreur, P.; Férey, G.; Morris, R. E.; Serre, C. Metal-Organic Frameworks in Biomedicine. *Chem. Rev.* **2012**, *112*, 1232−1268.
(13) Wu, M. X.; Yang, Y. W. Metal−Organic Framework (MOF)-Based Drug/Cargo Delivery and Cancer Therapy. *Adv. Mater.* **2017**, *29*, No. 1606134.
(14) Wang, T.; Farajollahi, M.; Henke, S.; Zhu, T.; Bajpe, S. R.; Sun, S.; Barnard, J. S.; Lee, J. S.; Madden, J. D. W.; Cheetham, A. K.; Smoukov, S. K. Functional Conductive Nanomaterials: Via Polymerisation in Nano-Channels: PEDOT in a MOF. *Mater. Horiz.* **2017**, *4*, 64−71.
(15) Sappia, L. D.; Tuninetti, J. S.; Ceolín, M.; Knoll, W.; Rafti, M.; Azzaroni, O. MOF@PEDOT Composite Films for Impedimetric Pesticide Sensors. *Global Challenges* **2020**, *4*, No. 1900076.
(16) Wang, B.; Côté, A. P.; Furukawa, H.; O'Keeffe, M.; Yaghi, O. M. Colossal Cages in Zeolitic Imidazolate Frameworks as Selective Carbon Dioxide Reservoirs. *Nature* **2008**, *453*, 207−211.
(17) Liang, K.; Ricco, R.; Doherty, C. M.; Styles, M. J.; Bell, S.; Kirby, N.; Mudie, S.; Haylock, D.; Hill, A. J.; Doonan, C. J.; Falcaro, P. Biomimetic Mineralization of Metal-Organic Frameworks as Protective Coatings for Biomacromolecules. *Nat. Commun.* **2015**, *6*, No. 7240.
(18) Hoop, M.; Walde, C. F.; Riccò, R.; Mushtaq, F.; Terzopoulou, A.; Chen, X. Z.; deMello, A. J.; Doonan, C. J.; Falcaro, P.; Nelson, B. J.; Puigmartí-Luis, J.; Pané, S. Biocompatibility Characteristics of the Metal Organic Framework ZIF-8 for Therapeutical Applications. *Appl. Mater. Today* **2018**, *11*, 13−21.
(19) Park, K. S.; Ni, Z.; Cote, A. P.; Choi, J. Y.; Huang, R.; Uribe-Romo, F. J.; Chae, H. K.; O'Keeffe, M.; Yaghi, O. M. Exceptional Chemical and Thermal Stability of Zeolitic Imidazolate Frameworks. *Proc. Natl. Acad. Sci. U.S.A.* **2006**, *103*, 10186−10191.
(20) Wang, P. L.; Xie, L. H.; Joseph, E. A.; Li, J. R.; Su, X. O.; Zhou, H. C. Metal-Organic Frameworks for Food Safety. *Chem. Rev.* **2019**, *119*, 10638−10690.
(21) Liédana, N.; Galve, A.; Rubio, C.; Téllez, C.; Coronas, J. CAF@ZIF-8: One-Step Encapsulation of Caffeine in MOF. *ACS Appl. Mater. Interfaces* **2012**, *4*, 5016−5021.
(22) Zhuang, J.; Kuo, C. H.; Chou, L. Y.; Liu, D. Y.; Weerapana, E.; Tsung, C. K. Optimized Metal-Organic-Framework Nanospheres for Drug Delivery: Evaluation of Small-Molecule Encapsulation. *ACS Nano* **2014**, *8*, 2812−2819.
(23) Lyu, F.; Zhang, Y.; Zare, R. N.; Ge, J.; Liu, Z. One-Pot Synthesis of Protein-Embedded Metal-Organic Frameworks with Enhanced Biological Activities. *Nano Lett.* **2014**, *14*, 5761−5765.
(24) Liang, W.; Xu, H.; Carraro, F.; Maddigan, N. K.; Li, Q.; Bell, S. G.; Huang, D. M.; Tarzia, A.; Solomon, M. B.; Amenitsch, H.; Vaccari, L.; Sumby, C. J.; Falcaro, P.; Doonan, C. J. Enhanced Activity of Enzymes Encapsulated in Hydrophilic Metal-Organic Frameworks. *J. Am. Chem. Soc.* **2019**, *141*, 2348−2355.
(25) Zhang, X.; Zhang, F.; Lu, Z.; Xu, Q.; Hou, C.; Wang, Z. Coupling Two Sequential Biocatalysts with Close Proximity into Metal-Organic Frameworks for Enhanced Cascade Catalysis. *ACS Appl. Mater. Interfaces* **2020**, *12*, 25565−25571.
(26) Liang, W.; Ricco, R.; Maddigan, N. K.; Dickinson, R. P.; Xu, H.; Li, Q.; Sumby, C. J.; Bell, S. G.; Falcaro, P.; Doonan, C. J. Control of Structure Topology and Spatial Distribution of Biomacromolecules in Protein@ZIF-8 Biocomposites. *Chem. Mater.* **2018**, *30*, 1069−1077.
(27) Lucock, M. Folic Acid: Nutritional Biochemistry, Molecular Biology, and Role in Disease Processes. *Mol. Genet. Metab.* **2000**, *71*, 121−138.
(28) Tamura, T.; Picciano, M. F. Folate and Human Reproduction. *Am. J. Clin. Nutr.* **2006**, *83*, 993−1016.
(29) Mitchell, L. E. Epidemiology of Neural Tube Defects. *Am. J. Med. Genet., Part C* **2005**, *135C*, 88−94.
(30) Dántola, M. L.; Urrutia, M. N.; Thomas, A. H. Effect of Pterin Impurities on the Fluorescence and Photochemistry of Commercial Folic Acid. *J. Photochem. Photobiol., B* **2018**, *181*, 157−163.
(31) Thomas, A. H.; Suárez, G.; Cabrerizo, F. M.; García Einschlag, F. S.; Martino, R.; Baiocchi, C.; Pramauro, E.; Capparelli, A. L. Photochemical Behavior of Folic Acid in Alkaline Aqueous Solutions and Evolution of Its Photoproducts. *Helv. Chim. Acta* **2002**, *85*, 2300−2315.
(32) Off, M. K.; Steindal, A. E.; Porojnicu, A. C.; Juzeniene, A.; Vorobey, A.; Johnsson, A.; Moan, J. Ultraviolet Photodegradation of Folic Acid. *J. Photochem. Photobiol., B* **2005**, *80*, 47−55.
(33) Kida, K.; Tomotake, M.; Sasako, H.; Matsuda, Y.; Sasaki, N.; Yamamoto, N. Small Amounts of Ethanol Attenuate Folic Acid Stability in Acidic Beverages during Storage. *Food Sci. Nutr.* **2018**, *6*, 214−219.
(34) Gazzali, A. M.; Lobry, M.; Colombeau, L.; Acherar, S.; Azaïs, H.; Mordon, S.; Arnoux, P.; Baros, F.; Vanderesse, R.; Frochot, C. Stability of Folic Acid under Several Parameters. *Eur. J. Pharm. Sci.* **2016**, *93*, 419−430.
(35) Dántola, M. L.; Denofrio, M. P.; Zurbano, B.; Gimenez, C. S.; Ogilby, P. R.; Lorente, C.; Thomas, A. H. Mechanism of Photooxidation of Folic Acid Sensitized by Unconjugated Pterins. *Photochem. Photobiol. Sci.* **2010**, *9*, 1604−1612.
(36) Luzuriaga, M. A.; Benjamin, C. E.; Gaertner, M. W.; Lee, H.; Herbert, F. C.; Mallick, S.; Gassensmith, J. J. ZIF-8 Degrades in Cell Media, Serum, and Some—but Not All—Common Laboratory Buffers. *Supramol. Chem.* **2019**, *31*, 485−490.
(37) Zheng, H.; Zhang, Y.; Liu, L.; Wan, W.; Guo, P.; Nyström, A. M.; Zou, X. One-Pot Synthesis of Metal-Organic Frameworks with Encapsulated Target Molecules and Their Applications for Controlled Drug Delivery. *J. Am. Chem. Soc.* **2016**, *138*, 962−968.
(38) Chowdhuri, A. R.; Laha, D.; Pal, S.; Karmakar, P.; Sahu, S. K. One-Pot Synthesis of Folic Acid Encapsulated Upconversion Nanoscale Metal Organic Frameworks for Targeting, Imaging and PH Responsive Drug Release. *Dalton Trans.* **2016**, *45*, 18120−18132.
(39) Chowdhuri, A. R.; Das, B.; Kumar, A.; Tripathy, S.; Roy, S.; Sahu, S. K. One-Pot Synthesis of Multifunctional Nanoscale Metal-Organic Frameworks as an Effective Antibacterial Agent against

https://dx.doi.org/10.1021/acs.iecr.0c04905
Ind. Eng. Chem. Res. XXXX, XXX, XXX−XXX

Multidrug-Resistant *Staphylococcus aureus*. *Nanotechnology* **2017**, *28*, No. 095102.
(40) Dong, H.; Yang, G. X.; Zhang, X.; Meng, X.; Bin; Sheng, J. L.; Sun, X. J.; Feng, Y. J.; Zhang, F. M. Folic Acid Functionalized Zirconium-Based Metal−Organic Frameworks as Drug Carriers for Active Tumor-Targeted Drug Delivery. *Chem. - Eur. J.* **2018**, *24*, 17148−17154.
(41) Xiao, J.; Zhu, Y.; Huddleston, S.; Li, P.; Xiao, B.; Farha, O. K.; Ameer, G. A. Copper Metal-Organic Framework Nanoparticles Stabilized with Folic Acid Improve Wound Healing in Diabetes. *ACS Nano* **2018**, *12*, 1023−1032.
(42) Xu, J.; Wu, L.; Guo, T.; Zhang, G.; Wang, C.; Li, H.; Li, X.; Singh, V.; Chen, W.; Gref, R.; Zhang, J. A "Ship-in-a-Bottle" Strategy to Create Folic Acid Nanoclusters inside the Nanocages of γ-Cyclodextrin Metal-Organic Frameworks. *Int. J. Pharm.* **2019**, *556*, 89−96.
(43) Ceborska, M.; Kędra-Królik, K.; Kowalska, A. A.; Koźbiał, M. Comparative Study of Molecular Recognition of Folic Acid Subunits with Cyclodextrins. *Carbohydr. Polym.* **2018**, *184*, 47−56.
(44) Pagano, C.; Perioli, L.; Latterini, L.; Nocchetti, M.; Ceccarini, M. R.; Marani, M.; Ramella, D.; Ricci, M. Folic Acid-Layered Double Hydroxides Hybrids in Skin Formulations: Technological, Photochemical and in Vitro Cytotoxicity on Human Keratinocytes and Fibroblasts. *Appl. Clay Sci.* **2019**, *168*, 382−395.
(45) Allwood, M. C.; Martin, H. J. The Photodegradation of Vitamins A and E in Parenteral Nutrition Mixtures during Infusion. *Clin. Nutr.* **2000**, *19*, 339−342.
(46) Allegretto, J. A.; Giussi, J. M.; Moya, S. E.; Azzaroni, O.; Rafti, M. Synthesis and Characterization of Thermoresponsive ZIF-8@ PNIPAm- Co -MAA Microgel Composites with Enhanced Performance as an Adsorption/Release Platform. *RSC Adv.* **2020**, *10*, 2453−2461.
(47) Allegretto, J. A.; Iborra, A.; Giussi, J. M.; von Biderling, C.; Ceolín, M.; Moya, S.; Azzaroni, O.; Rafti, M. Growth of ZIF-8 MOF Films with Tuneable Porosity by Using Poly(1-vinylimidazole) Brushes as 3D Primers. *Chem. - Eur. J.* **2020**, *26*, 12388−12396.
(48) Kuhn, H. J.; Braslavsky, S. E.; Schmidt, R. Chemical Actinometry (IUPAC Technical Report). *Pure Appl. Chem.* **2004**, *76*, 2105−2146.
(49) Ipiña, A.; Castaño, C.; Dántola, M. L.; Thomas, A. H. Solar Radiation Exposure of Dihydrobiopterin and Biopterin in Aqueous Solution. *Sol. Energy* **2014**, *109*, 45−53.
(50) Vora, A.; Riga, A.; Alexander, K. Processes to Identify the Degradation Mechanism of a Solid Which Appears to Undergo a Complex Reaction: Folic Acid. *Instrum. Sci. Technol.* **2002**, *30*, 193−203.
(51) Hu, Y.; Kazemian, H.; Rohani, S.; Huang, Y.; Song, Y. In Situ High Pressure Study of ZIF-8 by FTIR Spectroscopy. *Chem. Commun.* **2011**, *47*, 12694−12696.
(52) Sun, C.; Sze, R.; Zhang, M. Folic Acid-PEG Conjugated Superparamagnetic Nanoparticles for Targeted Cellular Uptake and Detection by MRI. *J. Biomed. Mater. Res., Part A* **2006**, *78A*, 550−557.
(53) Sutton, C. C. R.; Da Silva, G.; Franks, G. V. Modeling the IR Spectra of Aqueous Metal Carboxylate Complexes: Correlation between Bonding Geometry and Stretching Mode Wavenumber Shifts. *Chem. - Eur. J.* **2015**, *21*, 6801−6805.
(54) Palacios, E. G.; Juárez-López, G.; Monhemius, A. J. Infrared Spectroscopy of Metal Carboxylates: II. Analysis of Fe(III), Ni and Zn Carboxylate Solutions. *Hydrometallurgy* **2004**, *72*, 139−148.
(55) Li, H.; Eddaoudi, M.; O'Keeffe, M.; Yaghi, O. M. Design and Synthesis of an Exceptionally Stable and Highly Porous Metal-Organic Framework. *Nature* **1999**, *402*, 276−279.
(56) Jankovi, B. Thermal Stability Investigation and the Kinetic Study of Folnak Degradation Process under Nonisothermal Conditions. *AAPS PharmSciTech* **2010**, *11*, 103−112.
(57) Dash, S. K.; Dash, S. S.; Chattopadhyay, S.; Ghosh, T.; Tripathy, S.; Mahapatra, S. K.; Bag, B. G.; Das, D.; Roy, S. Folate Decorated Delivery of Self Assembled Betulinic Acid Nano Fibers: A Biocompatible Anti-Leukemic Therapy. *RSC Adv.* **2015**, *5*, 24144−24157.
(58) Cabrera, M. I.; Alfano, O. M.; Cassano, A. E. Novel Reactor for Photocatalytic Kinetic Studies. *Ind. Eng. Chem. Res.* **1994**, *33*, 3031−3042.
(59) Serpone, N.; Salinaro, A. Terminology, Relative Photonic Efficiencies and Quantum Yields in Heterogeneous Photocatalysis. Part I: Suggested Protocol (Technical Report). *Pure Appl. Chem.* **1999**, *71*, 303−320.
(60) de Britto, D.; Pinola, F. G.; Mattoso, L. H. C.; Assis, O. B. G. Analysis of Thermal and Aqueous Suspension Stabilities of Chitosan Based Nanoencapsulated Vitamins. *Quim. Nova* **2016**, *39*, 1126−1130.
(61) Neves, D. A.; de Sousa Lobato, K. B.; Angelica, R. S.; Teixeira Filho, J.; de Oliveira, G. P. R.; Godoy, H. T. Thermal and in Vitro Digestion Stability of Folic Acid in Bread. *J. Food Compos. Anal.* **2019**, *84*, No. 103311.
(62) do Evangelho, J. A.; Crizel, R. L.; Chaves, F. C.; Prietto, L.; Pinto, V. Z.; de Miranda, M. Z.; Dias, A. R. G.; da Rosa Zavareze, E. Thermal and Irradiation Resistance of Folic Acid Encapsulated in Zein Ultrafine Fibers or Nanocapsules Produced by Electrospinning and Electrospraying. *Food Res. Int.* **2019**, *124*, 137−146.

https://dx.doi.org/10.1021/acs.iecr.0c04905
Ind. Eng. Chem. Res. XXXX, XXX, XXX−XXX